scientific reports

Check for updates

OPEN

Impedance mapping with high-density microelectrode array chips reveals dynamic heterogeneity of in vitro epithelial barriers

Alessandra Venz[1,2], Bastien Duckert[2], Liesbet Lagae[1,2], Saeedeh Ebrahimi Takalloo[2,3] & Dries Braeken[2,3]✉

Epithelial tissues in vitro undergo dynamic changes while differentiating heterogeneously on the culture substrate. This gives rise to diverse cellular arrangements which are undistinguished by conventional analysis approaches, such as transepithelial electrical resistance measurement or permeability assays. In this context, solid substrate-based systems with integrated electrodes and electrochemical impedance monitoring capability can address the limited spatiotemporal resolution of traditional porous membrane-based methods. This label-free technique facilitates local, continuous, long-term analysis of tissue barrier properties for organ-on-chip applications. Increasing spatial resolution requires small electrodes arranged in a dense array, known as high-density microelectrode arrays (HD-MEAs). Integrated with Complementary Metal Oxide Semiconductor (CMOS) technology for multiplexing and rapid impedance measurements, HD-MEAs can enable high spatiotemporal resolution assessments of epithelial tissues. Here, we used 16,384 CMOS-integrated HD-MEA chip with subcellular-sized electrodes (8 µm diameter, 15 µm pitch, patterned in 16 clusters each consisting of 1024 electrodes in a 32 × 32 matrix) and impedance sensing capability to monitor dynamic evolution of Caco-2 cells, such as their proliferation, barrier formation, and 3D structure development on the chip. Changes in impedance at the selected frequency of 1 kHz ($|Z|_{1kHz}$) enabled monitoring and analyzing the life cycle of Caco-2 cells grown on the HD-MEA chips (up to + 453% change after 7 days in culture). The $|Z|_{1kHz}$ maps of proliferating Caco-2 cells and the differentiating epithelial tissue developing 3D domes aligned with the corresponding optical images at cellular resolution, which demonstrates the capability of the chip in tracking the dynamic heterogeneity of Caco-2 tissues in a label free and real-time fashion. Importantly, $|Z|_{1kHz}$ maps acquired during chemically induced barrier disruption showed electrodes covered with 3D cell domes experienced a stronger decrease in impedance than those covered with adherent cells (-41% ± sd 10% against -16% ± sd 10%, respectively). This method could thus, in principle, enable detection of tissue barrier disrupting and modifying agents with higher specificity. Epithelial barrier function assays benefit from using HD-MEA impedance sensors due to their increased informativity and resolution, which will be of great value in future organ-on-chip platforms.

Keywords CMOS microelectrode arrays, MEA, Electrical impedance, Epithelial barrier, Caco-2 cells

The intestinal epithelial barrier plays a critical role in maintaining gut homeostasis by preventing the invasion of luminal agents and pathogens into the underlying tissues. Disruption of this barrier can trigger chronic pathologies such as Inflammatory Bowel Disease (IBD), which has a compounding prevalence of > 0.3% worldwide[1]. In their physiological state, adjacent epithelial cells create a continuous layer that restricts the passage of most hydrophilic solutes such as water, ions, and macromolecules[2]. Tight junctions, protein complexes formed between cells to seal the paracellular space, are the primary determinants of barrier function, but can experience functional changes determined by inflammation which compromise the barrier, thus inducing a leaky state[2,3]. In vitro models of the intestinal epithelial barrier make use of human epithelial cells and tissue, enabling relevant pre-clinical assays to monitor barrier function and investigate absorption and toxicology

[1]Biophysics Department, KU Leuven, Leuven, Belgium. [2]imec, Leuven, Belgium. [3]Saeedeh Ebrahimi Takalloo and Dries Braeken shared senior authors. ✉email: dries.braeken@imec.be

of compounds. Among many other cell lines, Caco-2 cells, derived from human colorectal adenocarcinoma, are widely used as a model of the intestinal epithelial barrier in vitro[4–6]. The integrity of epithelial barriers is conventionally studied by monitoring the permeation of fluorescent dyes and by measuring the Transepithelial Electrical Resistance (TEER) across the cell barrier cultured on top of a porous membrane[7]. TEER is commonly measured using systems such as EVOM™ with either EndOhm chamber or STX2/chopstick electrodes (World Precision Instrument, LLC) or CellZScope® (nanoAnalytics GmbH). In both systems, tissues are cultured on top of commercially available porous membranes, a.k.a. Transwells®, in a static condition where the cells do not experience any fluid flow[8]. Thanks to the rise of microfluidic organ-on-chip platforms equipped with integrated electrodes, the barrier function of tissues grown on porous membrane can be measured in a dynamic condition, where the cells are subjected to fluid shear stress[9,10].

Alternative to the systems based on porous membranes, cells can be cultured on top of an array of patterned electrodes on a solid substrate such as polycarbonate, glass or silicon[11,12]. Electrochemical Impedance Spectroscopy (EIS) or monitoring at a selected single frequency is used there to detect changes in resistive and capacitive properties of tissues caused by the biological activities of the cells cultured on the electrodes[13]. This is done in real-time with high temporal resolution to characterize biologically-relevant parameters, such as cell–cell adhesion and cell-substrate adhesion[14]. Electrical cell substrate impedance sensing (ECIS®, Applied Biophysics Inc.) systems and xCELLigence® real-time cell analysers (RTCA, ACEA Biosciences Inc.) are two popular solid substrate-based systems being used to monitor two-dimensional cellular behaviour. ECIS® chips consist of up to 40 gold electrodes with a diameter of ~ 250 µm, each hosting 50 to 100 cells. Similarly, xCELLigence® RTCA e-plates are equipped with arrays of interdigitated gold microelectrodes to monitor cell behaviour. Both systems have been widely used for various applications, such as monitoring of cellular micromotion[15], drug discovery[16,17], toxicology assays[18,19], and cell and tissue biology studies[20,21]. In such systems, increasing the spatial resolution to get more information on the cultured cells requires smaller electrodes, organized in denser arrays, and integrated with high-speed acquisition and multiplexing systems. This has been realized through complementary metal oxide semiconductor (CMOS) micro-electrode arrays (MEAs), which are interfacing integrated circuits and multiplexers with high-density micron-sized electrodes[22–25]. CMOS-MEAs were originally developed to study the electrophysiology of neural or cardiac cells[26–28] and were later used for studying and imaging proliferation of eukaryotic cells[29] and bacterial biofilms[30], their micromotion[31,32] and the development of tissues[12,23].

Here, we use a CMOS-integrated 16,384 electrode high-density MEA chip[22] as an in vitro model to characterize Caco-2 epithelial barrier formation and growth, corroborated with fluorescence microscopy. Exploiting the impedance data acquired at 1 kHz ($|Z|_{1kHz}$) from 49,152 electrodes, we first demonstrate the stepwise process of cellular adhesion to the electrodes and subsequent tight junction formation between the cells, as well as differences between loss of cell adhesion and de-coupling of intercellular junctions. At a later stage of the life cycle of the epithelial barrier, we characterized the transformation from a two-dimensional to a three-dimensional tissue on the chip. Finally, using the high spatial resolution of the chip, we found that these epithelial barriers are not only showing heterogeneous growth dynamics, but also heterogenous response to disruption.

Materials and methods

Microelectrode arrays (MEA) chips

The CMOS HD-MEA chip (Fig. 1a) consists of 16,384 subcellular sized (8 µm in diameter) titanium nitride (TiN) electrodes with a pitch of 15 µm and a density of > 4000 electrodes/mm^2. The chips are fabricated as reported in[22] and packaged as in[28]. The 5×5 mm^2 cell-culture area of the chip (Fig. 1a, light blue square) is divided into 16 clusters, each arranged in a 32×32 matrix (1024 electrodes). All the 16,384 electrodes can be addressed individually. Around each cluster, eight electrodes with an area of 235×50 µm^2 are located to serve as the counter electrode.

The HD-MEA chips are interfaced with an in-house developed benchtop acquisition system, providing power to the chip, and connecting it to a computer. Utilizing a Graphical User Interface (GUI), users can select the proper cell interfacing modality among five: impedance monitoring, impedance spectroscopy, extracellular and intracellular voltage recording and voltage or current cell stimulation[22]. The system architecture of the impedance monitoring circuit is summarized in Fig. 1b, highlighting the recording channel, where the frequency and the amplitude of the excitatory current can be selected (1 kHz or 10 kHz and 1 nA or 10 nA, respectively). A reconfigurable instrumentation amplifier (Fig. 1b, grey triangle) records the resulting voltage on the electrode. Before cell seeding, the small variation in $|Z|_{1kHz}$ between electrodes ($|Z|_{1kHz}$ being equal to $0.26 \pm$ sd 0.03×10^6 Ω, Fig. 1b) confirms the uniform deposition and patterning of the TiN electrode, essential to perform reliable experiments[28,33].

Cell culture

An 8.4×8.4 mm^2 culture insert (Ibidi GmbH, Munich, Germany) was glued with EA M-31 CL epoxy (Loctite) around the dedicated cell culture area on the chip (Fig. 1a), which were then sterilized as described previously[34]. Chips were coated with 300 µl solution of Collagen Type1 Rat Tail (Corning) diluted in 0.02 N Acetic Acid (Merck) to 0.1 mg/ml. Carcinoma Colon-2 (Caco-2) cells ([Caco2] HTB-37™, ATCC) were seeded with a density of 50 k cells/ml, and incubated overnight at 37 °C with 5% CO_2. Cells were cultured on the chip in Eagle's Minimum Essential Medium (EMEM) medium (ATCC 30–2003#), supplemented with 20% Fetal Bovine Serum (FBS) (Biowest S.A.S.) and 1% penicillin/streptomycin (Merck) refreshed every day before the impedance measurements.

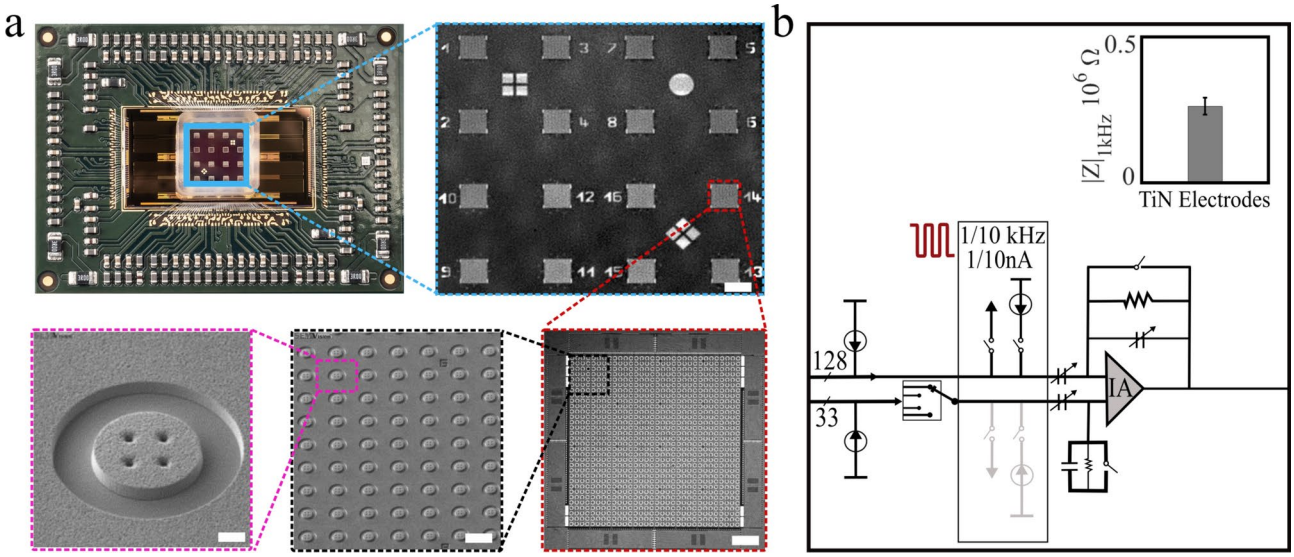

Fig. 1. **a**) Top left: top view optical photograph of the HD-MEA chip, highlighting the cell culture area in light blue. Top right: Confocal image of the 5×5 mm^2 cell culture area of the chip, demonstrating the 16 microelectrode clusters, one of which is highlighted with a red square; scale bar is 500 µm; Bottom right, confocal image of one cluster of electrodes, including an array of 32×32 microelectrodes, surrounded by 8 counter electrodes (235×50 µm^2); scale bar is 80 µm; Bottom middle, scanning electron microscopy (SEM) image of a section of the array of microelectrodes, showing the 15 µm pitch; scalebar is 15 µm; Bottom left, SEM image of a single TiN microelectrode (8 µm diameter); scale bar is 2 µm; **b**) System architecture of the impedance monitoring circuit of the HD-MEA chip; inset: mean $|Z|_{1kHz}$ for 16,384 electrodes on a single chip ($|Z|_{1kHz}$ being equal to $0.26 \pm 0.01 \times 10^6$ Ω);

Electrochemical impedance measurement

Impedance monitoring was carried out at 1 kHz (impedance magnitude denoted as $|Z|_{1kHz}$) by applying a 10 nA square wave current between each of the microelectrodes and the 8 counter electrodes surrounding the electrodes cluster. Within a frequency band ranging from 1 Hz to 100 kHz, a frequency of 1 kHz has been selected by using identical non-CMOS chips as it offers the largest difference in impedance after cell seeding and adhesion. For additional information on the process used for frequency selection see Supplementary Fig. 4. Impedance monitoring was performed before seeding the cells and every day after seeding for 14 days, at room temperature. A chip without cells was used as control for impedance measurement consistency. Other experiments of continuous impedance monitoring were carried out by applying 1 nA square wave current pulse every 20 min, at 37 °C. All impedance measurements were conducted in culture medium.

Barrier disruption

Experiments involving chemical disruption of tight junctions were conducted while measuring $|Z|_{1kHz}$ on the HD-MEA chip. For each experiment 50 k/cm^2 Caco-2 cells were seeded and cultured for 12 days. Caco-2 cell barrier was exposed to 5 mM Ethylene glycol-bis(2-aminoethylether)-N,N,N',N'-tetraacetic acid (EGTA) in Dulbecco's Modified Eagle Medium/Nutrient Mixture F-12 without phenol red (DMEM/F12, Gibco) without FBS, for 45 min at 37 °C. The recovery of the barrier was monitored by $|Z|_{1kHz}$ measurement after 24 h. To study treatment and recovery live imaging with CellMask^{TM} Plasma Membrane Staining (Invitrogen^{TM}), 1:1000 was applied in DMEM/F12 without FBS on the chip where impedance measurements were taken. Cells on two other chips were fixed (Fixative solution paraformaldehyde 4%, Invitrogen^{TM}) for immunostaining of Zonula Occludens 1 (ZO-1-1A12, Invitrogen^{TM}) before and after EGTA treatment.

Imaging

Optical and confocal images were done using a VHX7000 optical microscope (Keyence) and an LSM 780 (Zeiss) confocal microscope, respectively. Epifluorescence imaging was performed on an Axio Examiner Z1 microscope equipped with a humidified incubation chamber heated to 37 °C.

Statistical analysis

All the data were plotted using Matlab® 2022a software. Wilcoxon signed rank test was calculated in Matlab® to determine statistical significance with a 95% confidence interval (sample size of N = 1024), after the non-normal distribution of the data was assessed with Kolmogorov–Smirnov test. Wilcoxon sum rank test was instead used when comparing samples with different sizes in barrier disruption experiment. When reporting the percentage of decrease in the value of $|Z|_{1kHz}$, the impedance of the bare electrodes, measured before cell seeding, was subtracted to only reflect cell dependent changes.

Results and discussion

Impedance mapping of cell attachment and proliferation with single cell resolution using HD-MEA chips

The CMOS-integrated multiplexers and impedance monitoring circuitry on HD-MEA chips with electrodes of 8 µm in diameter and 15 µm pitch allow for impedance mapping to monitor Caco-2 cell adhesion and growth. After seeding the cells on the chip, the impedance monitoring correlated well with the corresponding brightfield and fluorescence images of cell localization. Figure 2a shows the $|Z|_{1kHz}$ map and microscope images of a cluster of 32 × 32 electrodes, 5 h, 24 h (day in vitro 2, DIV2) after seeding on chip. Only electrodes covered with cells display higher impedance, allowing us to create an 'impedance map' of the cell culture. This not only provides a comprehensive understanding of the cell culture dynamics, but also offers valuable insights into the extent and uniformity of cell coverage across the entire electrode area. Moreover, a single, label-free measurement using the HD-MEA system across all 16,384 electrodes only takes 7 minutes, while confocal microscopy requires labelling of cells, and the imaging itself requires about 30 minutes [28,35], decreasing drastically the assay time.

Life cycle monitoring of Caco-2 cells using HD-MEA chips

Caco-2 cells in vitro undergo barrier formation and start differentiating into enterocytes, as demonstrated previously through labelling and imaging methods[36–38]. We showed that the HD-MEA chip allows for fast, label-free, and high-resolution mapping of cell growth. We demonstrated a strong correlation between 2D impedance maps and cell coverage during early attachment phases (DIV1-2, Fig. 2). Next, we investigated long-term tracking of impedance changes over time. To do so, we performed daily $|Z|_{1kHz}$ measurements on Caco-2 cells for 14 consecutive days to investigate their long-term cellular behavior on the chips (Fig. 3). We discovered three distinctive cell growth phases that can be studied in detail with the HD-MEA chip.

The first phase, highlighted with a blue background in Fig. 3a, corresponds to cell attachment, spreading and barrier formation. In this phase, changes in impedance magnitude measured with the HD-MEA are mainly due to the decrease of cell-electrode distance, which is correlated to cell-substrate adherence[39]. At DIV2, the mean increase in $|Z|_{1kHz}$ is 214% with a large distribution (sd = ± 153%). This large distribution can be explained by the large variation exhibit by cells interacting with the chip surface at this stage. Electrodes showing no change in impedance (located at the bottom of the graph with $\Delta|Z|_{1kHz} \sim 0\%$) are not covered with cells yet. Other electrodes showing discernible increase in impedance with a heterogeneous distribution, represent cells that completely and partially adhered to the substrate. As previously shown in literature, strongly adhering cells cause a drastic relative increase in impedance[40,41]. Finally, the electrodes demonstrating the relative highest $\Delta|Z|_{1kHz}$ presumably represent cells that started to form tight junctions. Cells which develop intercellular tight junctions block the paracellular current flow more efficiently, leading to higher impedance magnitudes[37]. During the rest of the culture time in phase 1 (DIV3- DIV6), the impedance shows a steady increase on all measured electrodes, and a decrease in variability (sd = ± 146% at DIV6). The cells grow in number, reduce their width, and increase their height[4]. Around DIV6-7, the two-dimensional barrier is formed on the chip as demonstrated by the highest impedance magnitude observed along the Caco-2 cell life cycle (453% at DIV7).

In the second phase (Fig. 3a, middle section with a cyan background), the mean $\Delta|Z|_{1kHz}$ starts to decrease from 453% at DIV7 to 374% at DIV10. Caco-2 cells cultured on non-porous substrates and in static condition form structures called domes[37,42], which indicates Caco-2 cell polarization and differentiation to enterocytes[36–38,42]. Cells activate ionic pumps on their apical side and pump water and ions to their basal side, inflating the impermeable epithelial layer from the substrate[36,38,43]. During dome formation cells progressively

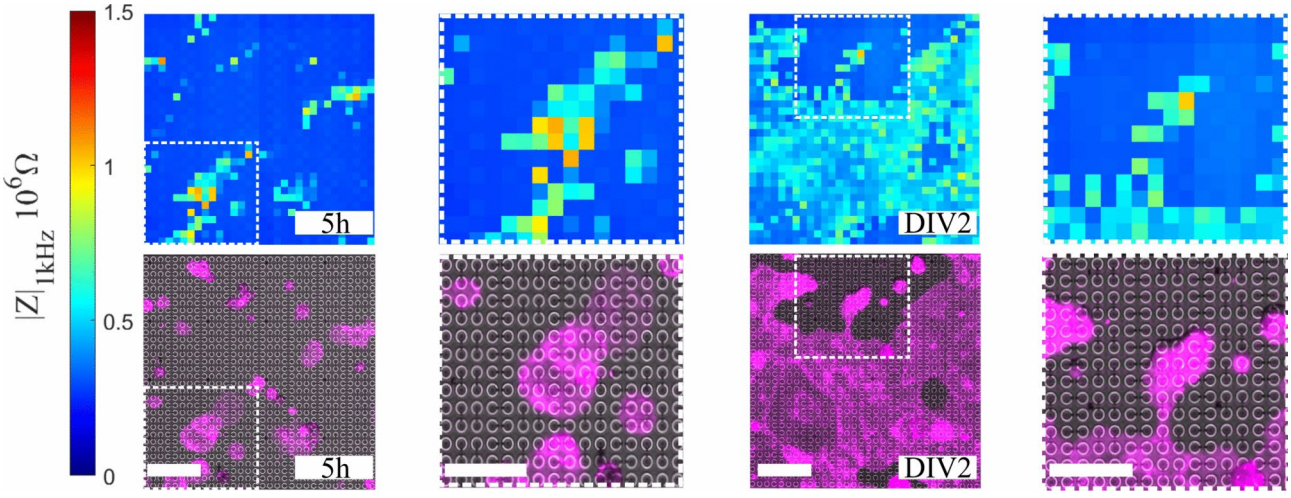

Fig. 2. Impedance map of the Caco-2 cell culture (40 k cells/cm^2) on the HD-MEA chip. Top:$|Z|_{1kHz}$ map of the 32 × 32 cluster of electrodes; from left to right: 5 h after seeding, and DIV2. Bottom: corresponding brightfield image of the chip overlayed with fluorescent cell membrane staining (magenta, bottom), matching the corresponding impedance mapping; scale bar is 100 µm; -contoured insets: enlarged area of the impedance map and corresponding microscope image.

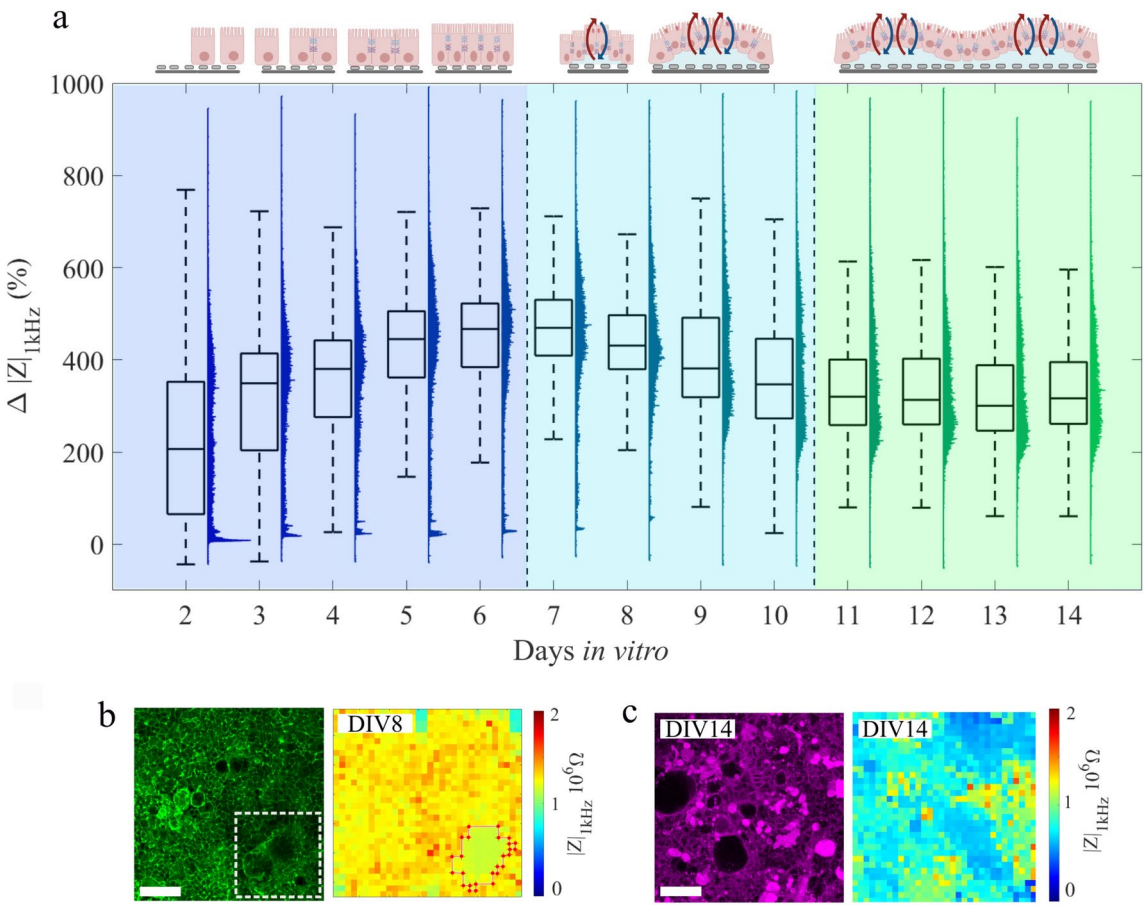

Fig. 3. **a**) Normalized change in $|Z|_{1kHz}$ of Caco-2 cells cultured on three HD-MEA chips (n = 49,152 electrodes; three biological repeats) over 14 days, demonstrating their life cycle. The normalization was done with respect to $|Z|_{1kHz}$ of the electrodes (= ~ 0.2–0.5 × 10^6 Ω) before cell seeding. The graph demonstrates three phases of Caco-2 cell barrier evolution: cell attachment, proliferation, and barrier formation (DIV0 to DIV6), initial formation of 3D domes (DIV7 to DIV10), and 3D domes expansion (DIV11 to DIV14). Cartoon styled illustration above the graph depicts a visual summary of the cell state throughout the three phases; bottom panel: representative impedance maps and microscopic images for different timepoints correlating $|Z|_{1kHz}$ of one of the 32 × 32 cluster of electrodes (right) and corresponding confocal images (left) of ZO-1 staining (**b**, green) of Caco-2 cells demonstrating the presence of a dome on the HD-MEA chip at DIV8, detected on the 2D impedance map (dashed rectangle, dome edge in red contour) and cell membrane staining in magenta at DIV14 (**c**); Scale bar is 100 µm.

detach from the electrodes as they are elevated by the fluid cumulated underneath the impermeable cell layer. Consequently, impedance drops with an increased rate of dome formation[36]. Finally, from DIV11, the progressive differentiation of the whole cell layer induces the shift to the third phase of the life cycle (Fig. 3a, right panel, with a green background). The $|Z|_{1kHz}$ plateau from DIV11 to DIV14 is representative of the epithelium fully developed in the third dimension. Starting from DIV8, domes increase in size and become easily detectable via fluorescence microscopy and $|Z|_{1kHz}$ mapping (Fig. 3b). On the HD-MEA, the electrodes under the dome area (inside red contour, Fig. 3b) measure a decreased $|Z|_{1kHz}$ (~ -7% on average compared to $|Z|_{1kHz}$ measured before dome formation) while the surrounding electrodes keep displaying a higher $|Z|_{1kHz}$ (~ -3% on average). This is coherent with what is reported in Chitale et al., which identifies a circular area of decreased impedance corresponding to dome location in Caco-2 formed epithelial tissue[44]. Tight junctions are still being expressed on the domes at this stage (ZO-1 staining, green, Fig. 3b and Supplementary Video S1), indicating the fact that the $|Z|_{1kHz}$ decrease is due to the cells detaching from the electrodes. At DIV15, the increased number of domes is detected on the impedance map as a decreased $|Z|_{1kHz}$ on most of the cluster's surface (Fig. 3c). Importantly, $|Z|_{1kHz}$ values at this stage are still larger than bare electrodes ($\Delta|Z|_{1kHz}$ DIV11 to 14 ~ 300% compared to baseline of bare electrodes). Moreover, as can be appreciated in Supplementary Fig. 2, within the plateau, electrodes covered by domes can be clearly visualized. There, the value of $|Z|_{1kHz}$ changes dynamically with the location of the domes.

Dynamic heterogeneity of Caco-2 epithelial barrier undergoing differentiation

Domes are dynamically interconnected by the continuous differentiation of the cells[36] as also appreciable from Fig. 4c bottom; the consequent changes in the hydraulic pressure of the cumulated liquid results in dynamic changes of domes locations, which make the tissue layer being elevated over the entire surface. Domes can be detected as small as ~ 15 µm up to several hundreds of µm in diameter (Fig. 4a, left to right). Due to the increased distance between the electrodes and the differentiated tissue, $|Z|_{1kHz}$ demonstrates lower values compared to the earlier phases of the culture. Nevertheless, as shown in Fig. 4b on the impedance map (inside black box) and Supplementary Fig. 2, changes of dome locations are easily detectable using impedance mapping and important information about the spatial arrangement of the epithelium on HD-MEA chip can be derived. Moreover, domes are dynamically changing their size over the culture, starting with a single cell stretching and progressively recruiting surrounding cells (Fig. 4a), as well as their level of inflation. Figure 4b (left and middle panels) displays a small dome inflating and deflating over the span of 20 min, detected on a cluster of the HD-MEA chip and visible from the 2D impedance map as an increased $|Z|_{1kHz}$ when deflating. Finally, confocal Z stacks taken from an individual dome demonstrate their ability to elevate above the electrode surface, while still maintaining intact barrier properties as indicated by the tight junction staining (Fig. 4c, ZO-1, green).

Heterogeneous response to disruption of Caco-2 epithelial barrier

Epithelial barrier disruption in vitro is characterized by on the one hand loss of cell attachment to the surface and on the other hand loosening of intercellular junctions. However, the differentiated Caco-2 cell layer is very heterogeneous, as demonstrated in the above-mentioned experiments, with the appearance, movement, and collapse of three-dimensional domes in the tissue. We thus investigated whether disruption of the epithelial barrier shows a heterogeneous response that depends on the presence of domes. For instance, Ethylene glycol tetraacetic acid (EGTA) is a chelating agent that has a high affinity for calcium. EGTA makes the barrier leaky by disrupting intercellular junctions and mildening cell attachment to the electrodes through the chelation of free Ca^{2+}, which is essential to the function of cell–cell and cell-substrate adhesion proteins[45]. To that end, we treated the cells at DIV12 with EGTA (5 mM) for 45 minutes, which is considered a mild disruption[10].

Figure 5a shows epifluorescence images and their corresponding 2D impedance maps of Caco-2 cells grown on the HD-MEA chip, before (t = 0 minutes) and after (t = 45 minutes) EGTA-induced barrier disruption. Overall, as expected, there is a significant decrease in $|Z|_{1kHz}$ upon application of EGTA (paired t test, $p < 0.005$). The disruption of tight junctions, crucial for maintaining barrier integrity, is also shown through immunohistochemistry using ZO-1 staining, highlighting the rounder shape of the cells detached from one another (Supplementary Figure S3). On the contrary, after wash-out and recovery for 24 h, $|Z|_{1kHz}$ even further increased, as cells are continuously differentiating, and domes might disappear (Fig. 5c, "REC").

From the 2D impedance map in Fig. 5a, it can be noticed that for the electrodes partially covered by a dome, the decrease in $|Z|_{1kHz}$ after EGTA treatment is considerably larger compared to the surrounding area (mean of -41% vs -16%). This can also be appreciated in Fig. 5c, which shows the percentage of change in $\Delta|Z|_{1kHz}$ over different areas of the electrodes cluster. To further explain this effect, we mapped the data points from the electrodes under the dome area (Fig. 5b, red data points) on the complete electrode cluster, highlighting the impedance change of the electrodes under the dome over the monitored timepoint.

The much more pronounced effect of barrier disruption under a dome area can be explained by the fact that the current path from the electrodes on the chip to the reference electrode is only blocked by the continuous cell layer floating above them, held together by the tight junctions between the cells. In areas where there are no domes, cells are still attached to the electrode surface, so the impedance measurement readout is a combination of cell attachment to the surface and tight junctions between the cells. When tight junctions are loosened by

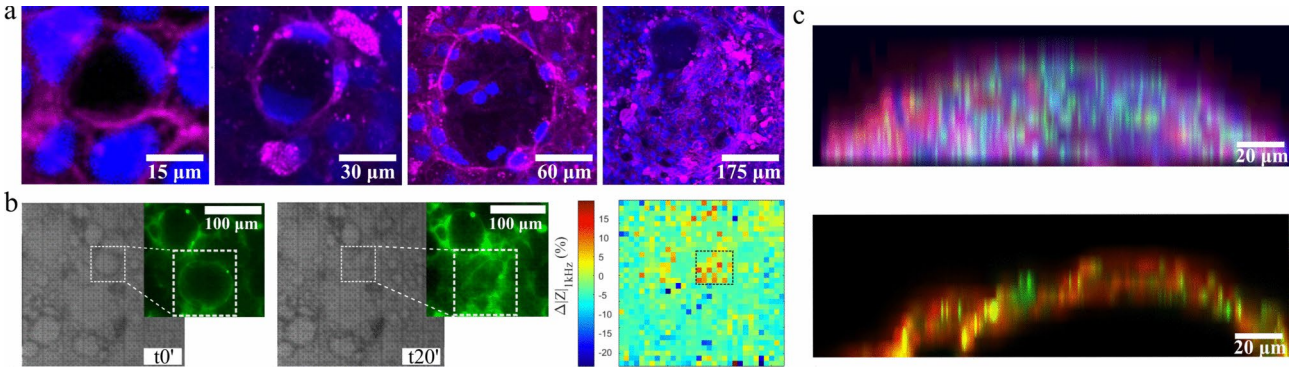

Fig. 4. Formation and rearrangement of three-dimensional domes of the Caco-2 cells on the HD-MEA chip. **a**) Confocal microscopic images of domes forming on chip; from left to right: single cell to multicellular 3D structures; nuclear staining is displayed in blue, cell membrane staining is displayed in magenta; **b**) Left and middle panel: brightfield image of an electrode cluster at DIV7 showing domes growing on the chip surface (left: t = 0; right: t = 20 min) and corresponding FITC-dextran live staining (insets); Right panel: relative impedance change over 20 min of a dome represented by the $\Delta|Z|_{1kHz}$ impedance; **c**) cross section of a dome at DIV8; blue is DAPI nuclear staining, red is f-actin staining, green is ZO-1 staining.

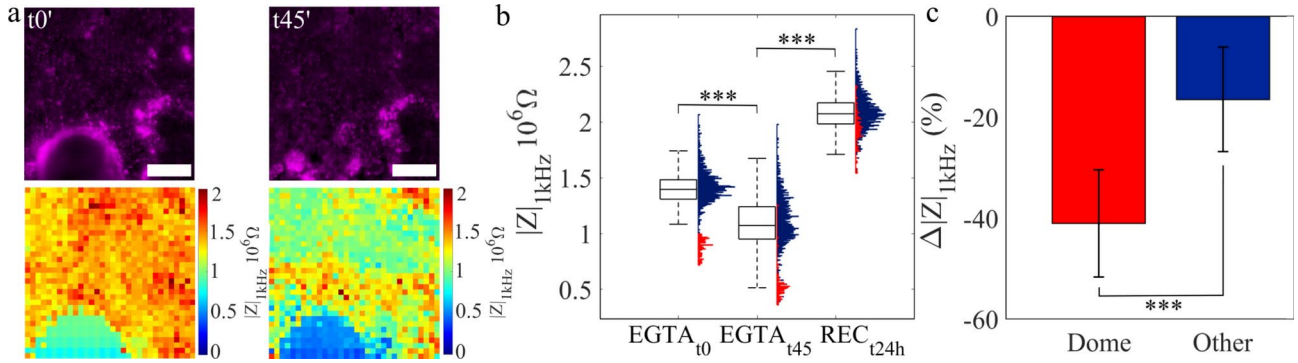

Fig. 5. **a**) Visualization of EGTA-induced barrier disruption through epifluorescence microscope imaging (top) and impedance mapping on a cluster of electrodes on the HD-MEA chip (bottom); a dome present on the bottom left of the cluster before treatment with EGTA is visible both in the fluorescence microscopy image and the impedance map (left images) 45 min after treatment (right images), however, the dome and is not visible on the fluorescence image anymore while it remains detectable through impedance mapping; Scalebar is 100 µm; **b**) Boxplot and histograms of $|Z|_{1kHz}$ for the electrode cluster under treatment highlighting the different electrode populations: electrodes under the dome area (red), values $< 1 \times 10^6\ \Omega$ at t_0 (a,left), and the other electrodes of the cluster (blue); Wilcoxon signed rank test, $p < 0.001$ for all conditions; **c**) Corresponding percentage of change in $|Z|_{1kHz}$ of different electrodes showing larger changes in those located under the dome (Wilcoxon sum rank test $p < 0.001$).

EGTA, the current path is still blocked by the cell adhering to the surface. This effect is thus dependent on the cell heterogeneity but marks an important differential experimental outcome. The latter experiment demonstrates the care that needs to be taken to understand the effects of barrier disruption when measured electrically using impedance methods. For example, in barrier disruption screenings, an agent that only temporarily loosens tight junctions can be wrongly considered as a strong barrier disruptor such as a cell death inducer, if the electrodes are covered with a dome at that moment. With larger electrodes and larger interelectrode distances, these effects can be easily missed or averaged out. Thus, care needs to be taken when traditional impedance monitoring systems are used for the analysis of barrier function in highly dynamic tissues in vitro. Similarly, live fluorescence staining of the cell layer yielded limited information about the degree and the patterning of tight junction loosening. On the contrary, impedance mapping on a HD-MEA could detect the complex behavior of cell domes with exquisite spatiotemporal resolution.

Conclusions

High-density microelectrode arrays have emerged as a promising technology to study cell behavior with high spatial and temporal resolution. In our study, we investigated the use of HD-MEA chips for label-free monitoring of epithelial cell growth and tissue dynamics through impedance mapping.

We demonstrated that impedance mapping with high spatial resolution reveals cellular information that is comparable to optical (fluorescence) imaging. The high-density electrode configuration enabled precise detection of cell attachment, spreading, and barrier formation. Secondly, we monitored Caco-2 cells for 14 days with impedance measurements and were able to describe the complete life cycle of the epithelial barrier in vitro, including attachment, barrier formation and cell differentiation. Using this approach, we discovered that Caco-2 barriers are extremely heterogeneous spatially but also temporally. Three-dimensional structures called domes appear and disappear over minutes and can range in size and height.

Moreover, we demonstrated that interpretation of barrier disruption using impedance strongly depends on the type and state of the cells growing atop the electrodes. This finding might have implications for the correct interpretation of barrier disruptor screening.

Finally, this work could contribute to the design of new human cell-based platforms and accelerate drug development for gastrointestinal diseases such as inflammatory bowel disease (IBD) and colorectal cancer. Overall, HD-MEA technology represents a unique addition to the existing range of methods for investigating epithelial and other tissue barrier functions.

Data availability

The datasets used and analyzed during the current study available from the corresponding author on reasonable request.

Received: 25 April 2024; Accepted: 6 January 2025
Published online: 10 January 2025

References

1. Ng, S. C. et al. Worldwide incidence and prevalence of inflammatory bowel disease in the 21st century: a systematic review of population-based studies. *Lancet* **390**(10114), 2769–2778. https://doi.org/10.1016/S0140-6736(17)32448-0 (2017).

2. Odenwald, M. A. & Turner, J. R. The intestinal epithelial barrier: A therapeutic target?. *Nat. Rev. Gastroenterol. Hepatol.* **14**(1), 9–21 (2017).
3. Bruewer, M. et al. Proinflammatory cytokines disrupt epithelial barrier function by Apoptosis-Independent mechanisms. *J. Immunol.* **171**(11), 6164–6172 (2003).
4. Hidalgo, I. J., Raub, T. J.,& Borchardt, R.T., Characterization of the Human Colon Carcinoma Cell Line (Caco-2) as a Model System for Intestinal Epithelial Permeability Gastroenterology. **96**, 736–749, 1989—The Backstory. Gastorenterology. *http://www.springerlink.com/index/* https://doi.org/10.1208/s12248-011-9283-8.
5. Gamboa, J.M., Leong, K.W. In vitro and in vivo models for the study of oral delivery of nanoparticles. *Adv Drug Deliv Rev.*;**65**(6):800–10. https://www.sciencedirect.com/science/article/pii/S0169409X13000306 (2013)
6. Raimondi, M. T., Albani, D. & Giordano, C. An Organ-On-A-Chip engineered platform to study the Microbiota–Gut–Brain axis in neurodegeneration. *Trends Mol. Med.* **25**(9), 737–740. https://doi.org/10.1016/j.molmed.2019.07.006 (2019).
7. Bednarek, R. In vitro methods for measuring the permeability of cell monolayers. *Methods Protoc* https://doi.org/10.3390/mps5010017 (2022).
8. Benson, K., Cramer, S. & Galla, H. J. Impedance-based cell monitoring: Barrier properties and beyond. *Fluids Barriers CNS.* **10**(1), 1–11 (2013).
9. Srinivasan, B. et al. TEER measurement techniques for in vitro barrier model systems. *J. Lab. Autom.* **20**(2), 107–126 (2015).
10. Henry, O. Y. F. et al. Organs-on-chips with integrated electrodes for trans-epithelial electrical resistance (TEER) measurements of human epithelial barrier function. *Lab. Chip.* **17**(13), 2264–2271 (2017).
11 Hierlemann, B. A., Frey, U., Hafizovic, S. & Heer, F. Growing cells atop microelectronic chips. *Proc. IEEE* https://doi.org/10.1109/JPROC.2010.2066532 (2011).
12 Bounik, R., Cardes, F., Ulusan, H., Modena, M. M. & Hierlemann, A. Impedance imaging of cells and tissues design and applications. *BME Front.* https://doi.org/10.34133/2022/9857485 (2022).
13. Stolwijk, J. A., Matrougui, K., Renken, C. W. & Trebak, M. Impedance analysis of GPCR-mediated changes in endothelial barrier function: overview and fundamental considerations for stable and reproducible measurements. *Pflugers Arch. Eur. J. Physiol.* **467**(10), 2193–2218 (2015).
14. Hucklesby, J. J. W. et al. Comparison of leading biosensor technologies to detect changes in human endothelial barrier properties in response to pro-inflammatory tnfα and il1β in real-time. *Biosensors.* **11**(5), 1–13 (2021).
15 Chiu, S. P. et al. Application of ECIS to assess FCCP-induced changes of MSC micromotion and wound healing migration. *Sensors (Switzerland)* https://doi.org/10.3390/s19143210 (2019).
16. Bushra, S. et al. Adiponectin ameliorates hyperglycemia-induced retinal endothelial dysfunction, highlighting pathways, regulators, and networks. *J. Inflamm. Res.* **15**(May), 3135–3166 (2022).
17. Johnson, R. H., Kho, D. T., O'Carroll, S. J., Angel, C. E. & Graham, E. S. The functional and inflammatory response of brain endothelial cells to Toll-Like Receptor agonists. *Sci. Rep.* **8**(1), 1–12 (2018).
18 Gueguen, E. et al. Endothelial barrier disruption by lipid emulsions containing a high amount of n3 fatty acids (Omegaven) but not n6 fatty acids (Intralipid). *Cells.* **11**(14), 2202 (2022).
19. Pan, T. et al. In vitro cytotoxicity assessment based on KC(50) with real-time cell analyzer (RTCA) assay. *Comput. Biol. Chem.* **47**, 113–120 (2013).
20. Mascarenhas, J. B. et al. An Actin-, Cortactin- and Ena-VASPLinked complex contributes to endothelial cell focal adhesion and vascular barrier regulation. *Cell Physiol. Biochem.* **56**(4), 329–339 (2022).
21. Shen, H. et al. ECIS-based biosensors for real-time monitor and classification of the intestinal epithelial barrier damages. *J. Electroanal. Chem.* https://doi.org/10.1016/j.jelechem.2022.116334 (2022).
22. Lopez, C. M. et al. A multimodal CMOS MEA for high-throughput intracellular action potential measurements and impedance spectroscopy in drug-screening applications. *IEEE J. Solid-State Circuits.* **53**(11), 3076–3086 (2018).
23. Abbott, J. et al. Multi-parametric functional imaging of cell cultures and tissues with a CMOS microelectrode array. *Lab. Chip.* **22**(7), 1286–1296 (2022).
24. Ballini, M. et al. A 1024-Channel CMOS microelectrode array with 26,400 electrodes for recording and stimulation of electrogenic cells in vitro. *IEEE J. Solid-State Circuits.* **49**(11), 2705–2719 (2014).
25. Park, JS., Grijalva, SI., Aziz MK., Chi. T., Li, S. Multi-parametric cell profiling with a CMOS quad-modality cellular interfacing array for label-free fully automated drug screening, *Lab a Chip - Miniaturisation Chem Biol.* http://feeds.rsc.org/~r/rss/LC/~3/uEPyjiNODhc/C8LC00156A (2018).
26. Müller, J. et al. High-resolution CMOS MEA platform to study neurons at subcellular, cellular, and network levels. *Lab. Chip.* **15**(13), 2767–2780 (2015).
27. Heer, F., Franks, W., Blau, A., Taschini, S., Ziegler, C., Hierlemann, A., et al. CMOS microelectrode array for the monitoring of electrogenic cells, *Biosens Bioelectron.* **20**(2):358–66 https://www.sciencedirect.com/science/article/pii/S0956566304000806(2004)
28 Miccoli, B. et al. High-density electrical recording and impedance imaging with a multi-modal CMOS multi-electrode array chip. *Front Neurosci.* **13**, 1–14 (2019).
29. Jung, D., Park, JS., Junek, G V., Grijalva, S I, Kumashi, S R, Wang, A., et al. A 21952-Pixel Multi-Modal CMOS Cellular Sensor Array with 1568-Pixel Parallel Recording and 4-Point Impedance Sensing. *IEEE Symp VLSI Circuits, Dig Tech Pap.;2019* C62–3 (2019)
30. Goikoetxea, E. et al. Impedimetric fingerprinting and structural analysis of isogenic E. coli biofilms using multielectrode arrays. *Sens. Actuators, B. Chem.* **263**, 319–326. https://doi.org/10.1016/j.snb.2018.01.188 (2018).
31. Dragas, J. et al. In vitro multi-functional microelectrode array featuring 59 760 electrodes, 2048 electrophysiology channels, stimulation, impedance measurement, and neurotransmitter detection channels. *IEEE J. Solid-State Circuits.* **52**(6), 1576–1590 (2017).
32. Mucha, A., Schienle, M. & Schmitt-Landsiedel, D. A CMOS integrated impedance-to-frequency converter for sensing cellular adhesion. *Adv. Radio Sci.* **9**, 281–287 (2011).
33 Jun, J. J. et al. Fully integrated silicon probes for high-density recording of neural activity. *Nature.* **551**(7679), 232–236. https://doi.org/10.1038/nature24636 (2017).
34 Duckert, B. et al. High-definition electroporation: Precise and efficient transfection on a microelectrode array. *J. Control Release* https://doi.org/10.1016/j.jconrel.2022.10.001 (2022).
35. Wegener, J., Keese, C. R. & Giaever, I. Electric cell-substrate impedance sensing (ECIS) as a noninvasive means to monitor the kinetics of cell spreading to artificial surfaces. *Exp. Cell Res.* **259**(1), 158–166 (2000).
36. Hara, A. Changes of proliferative activity and phenotypes in spontaneous differentiation of colon cancer cell lines. *JJ. Cancer Res.* **13**(1), 104–116 (1993).
37. Marziano, M. et al. Monitoring Caco-2 to enterocyte-like cells differentiation by means of electric impedance analysis on printed sensors. *Biochim. Biophys. Acta – Gen. Subj.* **1863**(5), 893–902 (2019).
38. Schreider, C., Peignon, .G., Thenet, S., Chambaz, J., Pinçon-raymond, M. Integrin-mediated functional polarisation of Caco-2 cells through E-cadherin-actin complexes (Schreider et al., Journal Cell Science, 2002).pdf>. 2002;
39 Giaever, I. & Keese, C. R. Micromotion of mammalian cells measured electrically. *Proc. Nat. Acad Sci.* **88**(17), 7896–7900 (1991).
40 Qiu, Y., Liao, R. & Zhang, X. Real-time monitoring primary cardiomyocyte adhesion based on electrochemical impedance spectroscopy and electrical cell– substrate impedance sensing. *Analyt. Chem.* **80**(4), 990–996 (2008).

41 Chen, Y. et al. Sensors and actuators B : Chemical short communication CMOS high density electrical impedance biosensor array for tumor cell detection. *Sens Actuators B. Chem.* https://doi.org/10.1016/j.snb.2012.07.024 (2012).
42. Pinto, M. Enterocyte-like differentiation and polarization of the human colon carcinoma cell line Caco-2 in culture. *Biol. Cell.* **47**, 323–330 (1983).
43 Latorre, E. et al. Active superelasticity in three-dimensional epithelia of controlled shape. *Nature.* **563**(7730), 203–208. https://doi.org/10.1038/s41586-018-0671-4 (2018).
44. Chitale, S. et al. A semiconductor 96-microplate platform for electrical-imaging based high-throughput phenotypic screening. *Nat. Commun.* **14**(1), 1–13 (2023).
45. Knipp, G.T, Ho, N.F.H, Barsuhn, C.L, Borchardt, R.T. Paracellular Diffusion in Caco-2 Cell Monolayers: Effect of Perturbation on the Transport of Hydrophilic Compounds That Vary in Charge and Size. *J Pharm Sci. 86*(10):1105–10. https://www.sciencedirect.com/science/article/pii/S0022354915503936(1997).

Acknowledgements

We would like to express our gratitude to Olga Krylychkina and Serena Pastore for helping with cell culture, Sophie Roth for Matlab® codes and Carolina Mora Lopez for chip and system design. We would extend our gratitude to Dennis Lambrechts, Marianne Carlon and Olivier Henry for the insightful discussions. The research in this paper was (co-)financed by the Research Foundation - Flanders (FWO file number S001221N).

Author contributions

Alessandra Venz: conceptualization, methodology, investigation, formal analysis, writing – original draft preparation, visualization. Bastien Duckert: methodology, investigation, resources, writing – original draft preparation. Saeedeh Ebrahimi Takalloo: conceptualization, formal analysis, visualization, writing – original draft preparation, supervision, project administration. Dries Braeken: conceptualization, formal analysis, writing -original draft preparation, visualization, supervision, funding acquisition, project administration. Liesbet Lagae: supervision and funding acquisition.

Declarations

Competing interests

There are no conflicts to declare.

Additional information

Supplementary Information The online version contains supplementary material available at https://doi.org/10.1038/s41598-025-85783-9.

Correspondence and requests for materials should be addressed to D.B.

Reprints and permissions information is available at www.nature.com/reprints.

Publisher's note Springer Nature remains neutral with regard to jurisdictional claims in published maps and institutional affiliations.

Open Access This article is licensed under a Creative Commons Attribution-NonCommercial-NoDerivatives 4.0 International License, which permits any non-commercial use, sharing, distribution and reproduction in any medium or format, as long as you give appropriate credit to the original author(s) and the source, provide a link to the Creative Commons licence, and indicate if you modified the licensed material. You do not have permission under this licence to share adapted material derived from this article or parts of it. The images or other third party material in this article are included in the article's Creative Commons licence, unless indicated otherwise in a credit line to the material. If material is not included in the article's Creative Commons licence and your intended use is not permitted by statutory regulation or exceeds the permitted use, you will need to obtain permission directly from the copyright holder. To view a copy of this licence, visit http://creativecommons.org/licenses/by-nc-nd/4.0/.

© The Author(s) 2025